

Quantum phase transitions in one-dimensional electron-phonon systems

HOLGER FEHSKE

Institut für Physik, Ernst-Moritz-Arndt-Universität Greifswald, 17487 Greifswald, Germany

ERIC JECKELMANN

Institut für Theoretische Physik, Universität Hannover, 30167 Hannover, Germany

1. – Introduction

Low dimensional strongly coupled electron-phonon systems like MX-chains, ferroelectric perovskites, conjugated polymers, or organic charge transfer salts exhibit a remarkable wide range of strengths of competing forces and, as a result, physical properties [1].

Most notably quasi one-dimensional (1D) materials are very susceptible to structural distortions driven by the electron-phonon (EP) interaction. Probably the most famous one is the Peierls instability [2] of 1D metals: As the temperature is lowered the system creates a periodic variation in the carrier density by shifting the ions from their symmetric positions. For the half-filled band case this so-called charge density wave (CDW) is commensurate with the lattice, the unit cell doubles, and the system possesses a spontaneous broken-symmetry ground state. Since a static dimerisation of the lattice opens a gap at the Fermi surface the metal gives way to a Peierls insulator (PI) [see Fig. 1].

The on-site Coulomb interaction, on the other hand, tends to immobilise the charge carriers as well by establishing a Mott insulating ground state. The Mott insulator (MI) exhibits strong spin density wave (SDW) correlations but has continuous symmetry and therefore shows no long-range order in 1D. Then, of course, the question arises, whether the PI and MI phases are separated by one (or more than one) quantum critical point(s) at $T = 0$, and if so, how the cross-over is modified by quantum phonon effects.

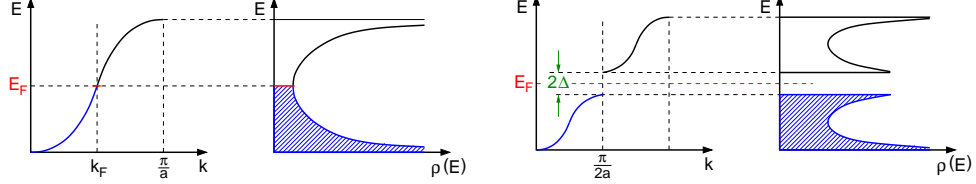


Fig. 1. – Peierls scenario: A gap 2Δ opens in the electronic band structure $E(k)$ [density of states $\rho(E)$] of an 1D metal if, as a result of the EP coupling, a static lattice distortion occurs, implicating a new lattice period $2a$ in real space.

The challenge of understanding such quantum phase transitions has stimulated intense work on generic microscopic models of interacting electrons and phonons like the Holstein Hubbard model (HHM):

$$(1) \quad H = -t \sum_{\langle i,j \rangle \sigma} c_{i\sigma}^\dagger c_{j\sigma} - g\omega_0 \sum_{i\sigma} (b_i^\dagger + b_i) n_{i\sigma} + \omega_0 \sum_i b_i^\dagger b_i + U \sum_i n_{i\uparrow} n_{i\downarrow}.$$

Here $c_{i\sigma}^\dagger$ ($c_{i\sigma}$) denote fermionic creation (annihilation) operators of electrons with spin $\sigma = \uparrow, \downarrow$ on a 1D lattice with N sites, $n_{i\sigma} = c_{i\sigma}^\dagger c_{i\sigma}$, and b_i^\dagger (b_i) are the corresponding bosonic operators for dispersionless optical phonons.

The physics of the HHM is governed by three competing effects: The itinerancy of the electrons ($\propto t$), their on-site Coulomb repulsion ($\propto U$), and the local EP coupling ($\propto g$). Since the EP interaction is retarded, the phonon frequency (ω_0) defines a further relevant energy scale. This advises us to introduce besides the adiabaticity ratio (ω_0/t) two dimensionless coupling constants ($u = U/4t$ and $\lambda = 2\varepsilon_p/2t$ or $g^2 = \varepsilon_p/\omega_0$).

In the single-electron case, the Holstein model [3] has been studied extensively as a paradigmatic model for polaron formation (see, e.g., Ref. [4]). Here ε_p gives the polaron

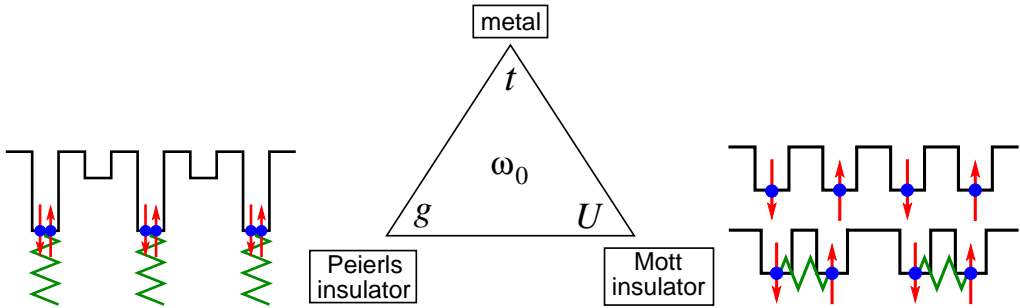


Fig. 2. – Schematic phase diagram of the 1D Holstein Hubbard model. At half-filling, Peierls (left) or Mott (right) insulating phases may be favoured over the metallic state. In the case of localised electrons interacting via antiferromagnetic exchange and magneto-elastic couplings even a spin-Peierls distorted state can emerge (right, lower panel).

binding energy. The Hubbard model [5], originally designed to describe ferromagnetism of transition metals, more recently has been in use in the context of metal-insulator transition and high-temperature superconductivity as the probably most simple model to account for strong Coulomb correlation effects. As yet there exists almost no exact (analytical) results for the full HHM (1). At least at half-filling, however, it has become generally accepted that the interplay of charge, spin and lattice degrees of freedom gives rise to the phase diagram sketched in Fig. 2. This scenario is supported by dynamical mean field investigations of the HMM, which become reliable at least in infinite spatial dimension [6]. Besides the properties of the ground state, the nature of the physical excitations is puzzling as well, especially in 1D. While one expects “normal” electron-hole pair excitations in the PI phase ($U = 0$), charge (spin) excitations are known to be massive (gapless) in the MI state of the Hubbard model ($\lambda = 0$). Thus, varying the control parameter u/λ , a cross-over from standard quasi-particle behaviour to spin-charge separation might be observed in the more general 1D HHM.

The aim of this contribution is to establish this physical picture and the anticipated phase diagram of the 1D HHM. For these purposes we employ the Lanczos exact diagonalisation (ED) [7, 8], kernel polynomial (KPM) [9, 10] and density-matrix renormalisation group (DMRG) [11] methods (see Jeckelmann/Fehske [12]). These numerical techniques allow us to obtain unbiased results for all interaction strengths with the full quantum dynamics of phonons taken into account.

2. – Luttinger-liquid Peierls-insulator transition

2.1. Holstein model of spinless fermions. – In a first step, let us neglect the spin degrees of freedom. The resulting 1D spinless Holstein model, $H = -t \sum_{\langle i,j \rangle} c_i^\dagger c_j - g\omega_0 \sum_i (b_i^\dagger + b_i)n_i + \omega_0 \sum_i b_i^\dagger b_i$, exhibits a quantum phase transition from a metallic to an insulating phase at half-filling ($N_e = N/2$) [13, 14], where the critical coupling $\lambda_c(\omega_0) \rightarrow 0$ for $\omega_0 \rightarrow 0$. In the anti-adiabatic ($\omega_0 \rightarrow \infty$) strong EP coupling regime, the model can be transformed to the exactly solvable XXZ (small polaron) model [13], which shows a transition of Kosterlitz-Thouless type. Various variational [15], renormalisation group [16], world-line quantum Monte Carlo [13] or Green’s-function Monte Carlo [17] methods were used to determine the phase boundary, within which significant discrepancies occur in the adiabatic intermediate coupling regime. More precise ED [18] and DMRG [19] techniques yields the phase diagram presented in Sec. 2.3.

2.2. Luttinger-liquid parameters and charge structure factors. – Before we discuss the metal insulator transition in the framework of the Holstein model we will characterise the metallic and insulating phases in themselves. According to Haldane’s LL conjecture [20], an 1D gapless (metallic) system of interacting fermions should belong to the Tomonaga-Luttinger universality class. Since the Holstein model of spinless fermions is expected to be gapless at weak couplings g , we try to determine the (non-universal) Luttinger liquid (LL) parameters, K_ρ (correlation exponent) and u_ρ (charge velocity), by performing a large-scale DMRG finite-size scaling analysis. To leading order, the ground-state energy

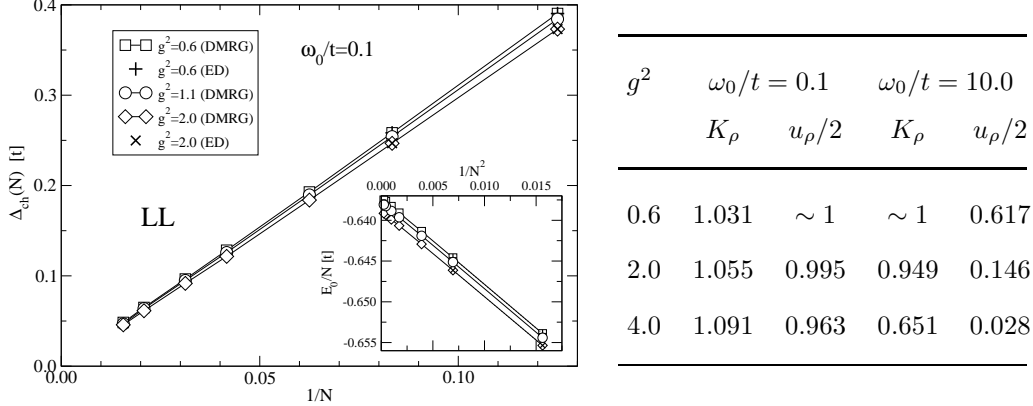


Fig. 3. – DMRG finite-size scaling of the charge gap $\Delta_c(N)$ and the ground-state energy $E_0(N)$. ED data included for comparison. The Table gives the LL parameters extracted from the scaling relations. Note that $K_\rho > 1$ ($K_\rho < 1$) in the adiabatic (anti-adiabatic) regime.

and the charge excitation gap of a finite system with N sites scales as:

$$(2) \quad \frac{E_0(N)}{N} = \varepsilon_0(\infty) - \frac{\pi}{3} \frac{u_\rho}{2} \frac{1}{N^2},$$

$$(3) \quad \Delta_c(N) = E_0^\pm(N) - E_0(N) = \pi \frac{u_\rho}{2} \frac{1}{K_\rho} \frac{1}{N}.$$

Here $\varepsilon_0(\infty)$ denotes the energy density of the infinite system with $N/2$ electrons, and $E_0^\pm(N)$ are the ground-state energies with ± 1 fermions away from half-filling.

The LL scaling relations (2) and (3) were derived for the pure electronic spinless fermion model only [21]. Figure 3 demonstrates, exemplarily for the adiabatic regime, that they also hold for the case that a finite EP coupling is included. The resulting LL parameters are specified in the Table. Interestingly the LL phase splits in two different regimes: For low phonon frequencies the effective fermion-fermion interaction is attractive ($K_\rho > 0$), while it is repulsive ($K_\rho < 0$) for high frequencies. In the latter region the kinetic energy ($\propto u_\rho$) is strongly reduced and the charge carriers behave like (small) polarons. In between, there has to be a point where the LL is made up of (almost) non-interacting particles ($K_\rho = 1$). The LL scaling breaks down just at the critical coupling $g_c(\omega_0/t)$, signalling the transition to the CDW state. We found $g_c^2(\omega_0/t = 0.1) \simeq 7.84$ and $g_c^2(\omega_0/t = 10) \simeq 4.41$.

Figure 4 proves the existence of CDW long-range order above g_c . Here the staggered charge structure factor

$$(4) \quad S_c(\pi) = \frac{1}{N^2} \sum_{i,j} (-1)^j \langle (n_i - \frac{1}{2})(n_{i+j} - \frac{1}{2}) \rangle$$

unambiguously scales to a finite value in the thermodynamic limit ($N \rightarrow \infty$). In contrast

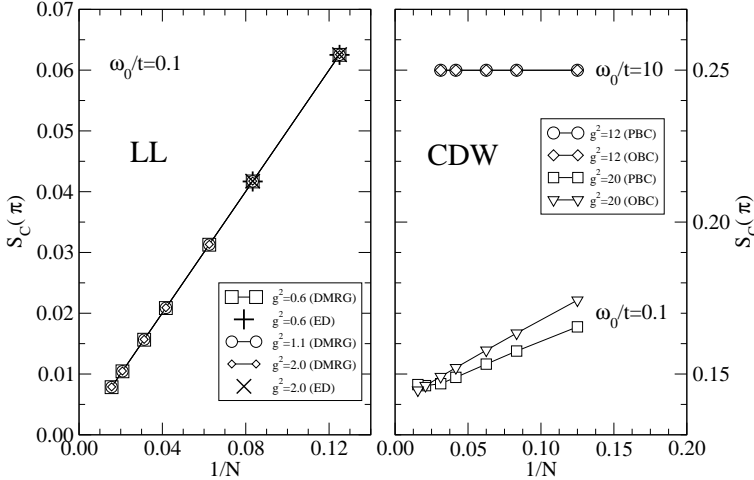


Fig. 4. – DMRG scaling of the charge structure factor $S_c(\pi)$ using periodic (PBC) and open (OBC) boundary conditions.

we have $S_c(\pi) \rightarrow 0$ in the metallic regime ($g < g_c$). Note that such a finite-size scaling, including dynamical phonons, is definitely out of the range of any ED calculation.

2.3. Phase diagram of the Holstein model of spinless fermions. – Figure 5 gives the position of the LL-CDW phase boundary in the $g-\omega_0^{-1}$ plane. For weak EP interactions the system is a metal with LL parameters depending on both the coupling strength and the phonon frequency. Increasing ω_0 at fixed g (which nonetheless means that the EP coupling parameter λ becomes larger) the cross-over from an attractive LL (adiabatic regime) to a repulsive LL (anti-adiabatic regime) takes place at about $\omega_0/t \simeq 1$. Keeping ω_0 fixed we enter the CDW phase at a critical EP coupling $g_c(\omega_0)$. ED, cluster perturbation theory [22] and projector-based renormalisation methods [23] reveals the softening of the optical phonon at the Brillouin-zone boundary, at least in the adiabatic regime, which can be understood as precursor effect of the gap formation. Note that in $D = \infty$, the opening of the electronic gap is accompanied by the appearance of a low-energy phonon peak in the total phononic spectral function [24].

The CDW for strong EP coupling is connected to a Peierls distortion of the lattice, and can be classified as traditional band insulator and polaronic superlattice in the strong-EP coupling adiabatic ($\omega_0/t \ll 1$) and anti-adiabatic ($\omega_0/t \gg 1$) regimes, respectively. Extremely valuable information about the CDW state can be obtained by analysing the regular part of the optical conductivity,

$$(5) \quad \sigma^{\text{reg}}(\omega) = \sum_{m>0} \frac{|\langle \psi_0 | i t \sum_j (c_j^\dagger c_{j+1} - c_{j+1}^\dagger c_j) | \psi_m \rangle|^2}{E_m - E_0} \delta[\omega - (E_m - E_0)],$$

which is connected due to finite-frequency optical transitions to excited quasi-particle states $|\Psi_m\rangle$. In Eq. (5), $\sigma^{\text{reg}}(\omega)$ is given in units of πe^2 and we have omitted an $1/N$ prefactor. The evaluation of dynamical correlation functions like $\sigma^{\text{reg}}(\omega)$ can be carried

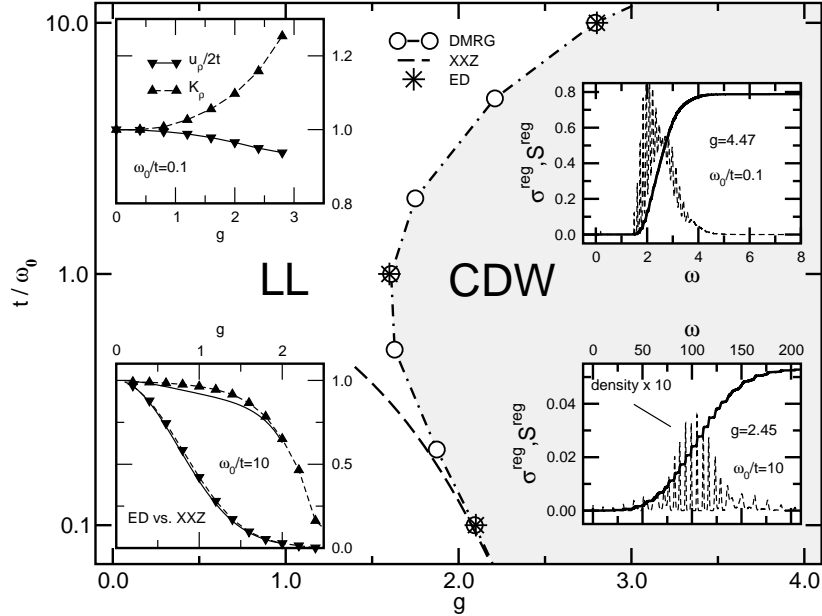


Fig. 5. – Ground-state phase diagram of the 1D half-filled Holstein model of spinless fermions, showing the boundary between the LL and CDW states obtained by ED and DMRG approaches. The dashed line gives the asymptotic result for the XXZ model. Left insets show the LL parameters u_p and K_p as a function of the EP coupling g in the metallic regime; right insets display for a six-site chain the regular part of the optical conductivity $\sigma^{\text{reg}}(\omega)$ (dotted lines) and the integrated spectral weight $S^{\text{reg}}(\omega) = \int_0^\omega d\omega' \sigma^{\text{reg}}(\omega')$ (solid lines) in the CDW region.

out by means of the very efficient and numerically stable ED-KPM algorithm [10]. The optical absorption spectra shown in Fig. 5 elucidate the different nature of the CDW for small and large adiabaticity ratios. In the adiabatic region the most striking feature is the sharp absorption threshold and large spectral weight contained in the incoherent part of optical conductivity. In the anti-adiabatic regime the CDW is basically a state of alternate self-trapped polarons, which means that the electrons are heavily dressed by phonons. Since the renormalised band dispersion is extremely narrow, finite-size gaps are reduced as well. Therefore, Δ_{opt} read off from Fig. 5 correctly gives the CDW gap.

3. – Peierls-insulator Mott-insulator transition

3.1. Ground-state properties. – Now we include the spin degrees of freedom and ask for the effect of a finite Coulomb interaction. The ground state of the pure Holstein model ($U = 0$) is a Peierls distorted state with staggered charge order, i.e. alternating empty and doubly occupied sites, for $g > g_c(\omega_0)$ [25, 26]. As in the Holstein model of spinless fermions, quantum phonon fluctuations destroy the Peierls state for $g < g_c$.

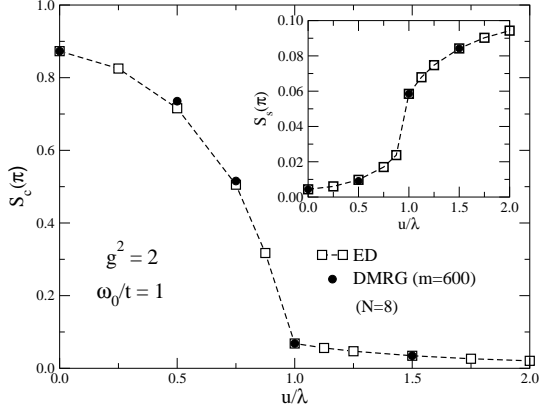


Fig. 6. – Spin and charge structure factors at $q = \pi$ in the half-filled 1D 8-site HHM (1) with PBC for different u at $\lambda = 1$. Squares denote ED results, filled circles show DMRG calculations with $m = 600$ target states and six pseudo-sites.

The charge structure factor, $S_c(\pi)$ [cf. Eq. (4)], and spin structure factor,

$$(6) \quad S_s(\pi) = \frac{1}{N^2} \sum_{i,j} (-1)^j \langle S_i^z S_{i+j}^z \rangle \quad \text{with} \quad S_i^z = \frac{1}{2} (n_{i\uparrow} - n_{i\downarrow}),$$

shown in Fig. 6 for the full HHM, indicate pronounced CDW and weak SDW correlations provided $u/\lambda < 1$. Increasing the Hubbard interaction u at fixed EP coupling λ

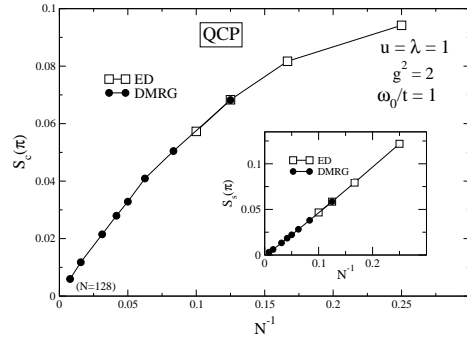
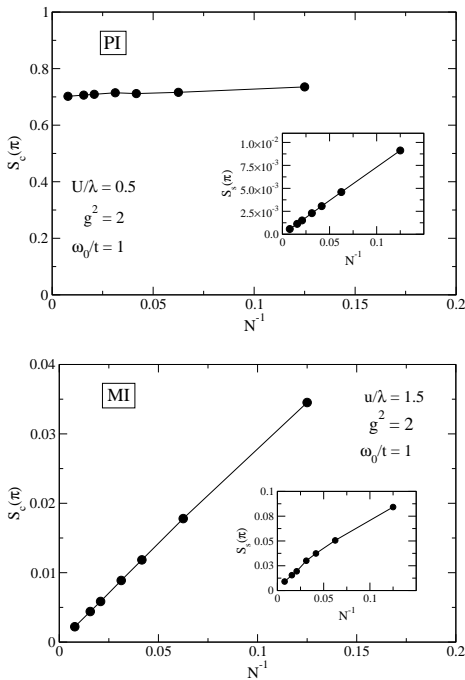


Fig. 7. – DMRG study of staggered charge and spin (inset) structure factors as a function of inverse lattice size in the PI and MI regimes, as well as at the quantum critical point (QCP). Generally, $m = 1000$ and 5 boson pseudo-sites were chosen for the DMRG algorithm, with the exception of the $N = 128$ case where $m = 800$ had to be used for practical reasons with no qualitative loss of accuracy.

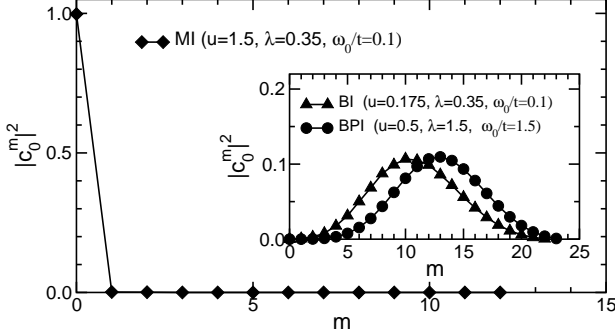


Fig. 8. – Phonon distribution, $|c_0^m|^2$, for typical model parameters characterising the MI, band insulator (BI) and bipolaronic insulator (BPI) Peierls phases (inset). Note that we have separated the $Q = 0$ centre of mass phonon.

and frequency ω_0 , the CDW correlations become strongly suppressed, whereas the spin structure factor at $q = \pi$ is enhanced.

The results depicted in Fig. 6 are obtained for a rather small eight-site chain with PBC. In order to conclude about a possible existence of charge and/or spin long-range order we have calculated $S_c(\pi)$ and $S_s(\pi)$ for different system sizes and performed a finite-size scaling of our DMRG results (see Fig. 7). In the PI phase, $S_c(\pi)$ shows almost no dependence on the size of the system, indicating true CDW long-range order, whereas $S_s(\pi)$ obviously scales to zero as $N \rightarrow \infty$. By contrast, in the MI regime our data provides strong evidence for vanishing charge but also spin order in the thermodynamic limit. Clearly the MI is characterised by short-ranged antiferromagnetic spin correlations but nevertheless the staggered spin-spin correlation function shows a slow (algebraic) decay at large distances.

Figure 8 gives the phonon distribution function, i.e. the weights of the m -phonon state for different ground states of the HHM. First of all the results demonstrate that our Hilbert space optimisation and truncation procedure is well-controlled in the sense that states with larger number of phonons, as accounted for in the calculations, have negligible spectral weight. Of course, the number of phonons which have to be taken into account depends on the physical situation. Whereas the ground state of the MI is basically a zero-phonon state, multi-phonon states become increasingly important if u/λ is reduced, i.e. in the PI state.

3.2. Optical response. – The evolution of the optical conductivity $\sigma^{\text{reg}}(\omega)$ going from the PI to the MI phase by increasing u/λ is illustrated in Fig. 9. In the PI regime the electronic excitations are gapped due to the CDW formation. Excitonic gap states may occur in the process of structural relaxation. Because the PI ground state is a multi-phonon state, we find a gradual rise of the integrated spectral weight of $\sigma^{\text{reg}}(\omega)$.

At the QCP the optical gap Δ_{opt} closes. Since we are in the non-adiabatic regime ($\omega_0 \simeq t$), the lowest optical excitations have mainly pure electronic character in the vicinity of $(u/\lambda)_c$, i.e. the gap is closed by a state having large electronic spectral weight. Due to the selection rules for optical transitions the PI-MI transition necessarily implies a ground-state level crossing with a site-parity change. The site inversion symmetry operator P is defined by $P c_{i\sigma}^\dagger P^\dagger = c_{N-i\sigma}^\dagger$ ($N = 4n$). We have explicitly verified that the

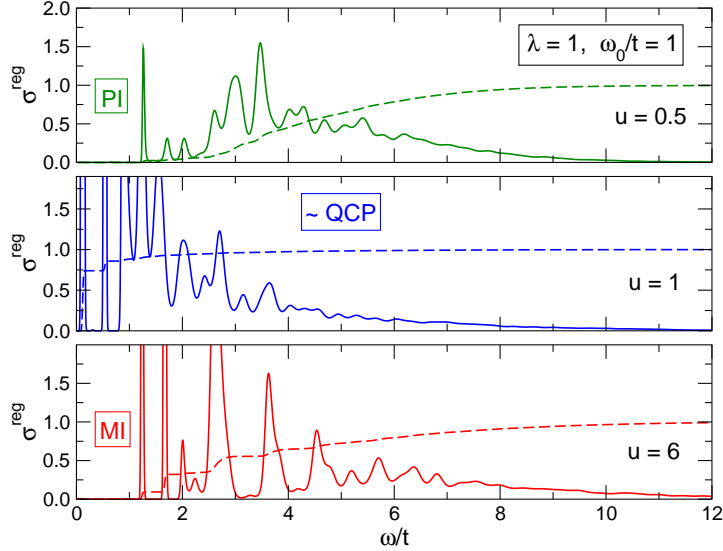


Fig. 9. – Optical conductivity in the Holstein Hubbard model (ED, $N = 8$, PBC). Dashed lines give the integrated spectral weight normalised by $S^{\text{reg}}(\infty)$. $S^{\text{reg}}(\omega)/S^{\text{reg}}(\infty)$ is a natural measure for the relative weight of the different optical absorption processes. Note that the critical coupling is identical to the point where $S_c(\pi)$ sharply drops (cf. Fig. 6).

parity is $P = +1$ ($P = -1$) in the PI (MI) phase.

In the MI the optical gap is by its nature a correlation gap. The lower panel in Fig. 9 shows clearly that $\sigma^{\text{reg}}(\omega)$ is dominated by excitations which can be related to those of the pure Hubbard model. In addition, phononic sidebands with low spectral weight appear.

3.3. Photoemission spectra. – Next we study the spectral density of single-particle excitations associated with the injection of a spin- σ electron with wave number K , $A_{K\sigma}^+(\omega)$ (inverse photoemission (IPE)), and the corresponding quantity for the emission of an electron, $A_{K\sigma}^-(\omega)$ (photoemission (PE)), where

$$(7) \quad A_{K\sigma}^\pm(\omega) = \sum_m |\langle \psi_m^\pm | c_{K\sigma}^\pm | \psi_0 \rangle|^2 \delta[\omega \mp (E_m^\pm - E_0)]$$

with $c_{K\sigma}^+ = c_{K\sigma}^\dagger$ and $c_{K\sigma}^- = c_{K\sigma}$. $|\psi_0\rangle$, E_0 refer to the ground state of the system with $N_e = N$ electrons and $|\psi_m^\pm\rangle$ (E_m^\pm) are eigenstates (energies) of the $(N_e \pm 1)$ -particle system. Adding the spectral densities of (photo-) emission and absorption we obtain the spectral function $A_{K\sigma}(\omega) = A_{K\sigma}^+(\omega) + A_{K\sigma}^-(\omega)$, which obeys various sum rules and allows for a connection to angle-resolved photoemission spectroscopy (ARPES).

Figure 10 displays the IPE and PE spectra for the HHM at the allowed wave numbers of our finite system: $K = 0, \pm\pi/4, \pm\pi/2, \pm 3\pi/4$, and π . To reliably monitor a band

splitting induced by the Hubbard and EP couplings it is necessary to guarantee that the Fermi momenta $K_F = \pm\pi/2$ are occupied, which is the case for $N = 4l$ (l integer, PBC).

The most prominent feature we observe in the PI regime is the opening of a gap at $K = \pm\pi/2$. For the BI a rather broad (I)PE signatures appear. Within these excitation bands the spectral weight is almost uniformly distributed, which is a clear signature of the multi-phonon absorption and emission processes that accompany every single-particle excitations in the PI. The lineshape reflects the (Poisson-like) distribution of the phonons in the ground state. The lower and upper band closely follow a (slightly renormalised) cosine dispersion. The situation changes radically if the insulating behaviour is associated with localised bipolarons forming a CDW state (see Fig. 10, upper right panel). Due to strong polaronic effects an almost flat band dispersion results with exponentially small (electronic) quasi-particle weight. Now the dominant peaks in the incoherent part of the (I)PE spectra are related to multiples of the (large) bare phonon frequency.

If we increase the Hubbard interaction at fixed EP coupling strength the Peierls gap weakens and finally closes at about $(u/\lambda)_c \simeq 1$, which marks the PI-MI cross-over. This is the situation shown in the lower left panel. Approaching the QCP, the ground state and the first excited state become degenerate. The QCP is characterised by gapless charge excitations at the Fermi momenta but perhaps should not be considered as metallic because the Drude weight in the case of a degenerate ground state is ill-defined [27].

If the Hubbard interaction is further increased, i.e. the Coulomb repulsion overcomes the attractive on-site EP coupling the electronic band structure becomes gapped again and a MI state develops (see lower right panel). The Mott-Hubbard correlation gap almost coincides with the optical gap Δ_{opt} determined by evaluating the regular part of the optical conductivity for the same parameters. The form of the spectra, however, is quite different from PI case. Contrary to the BI phase in the MI regime the lowest peak in each K sector is clearly the dominant one. Then the dispersion of the lower (upper) Hubbard band can be derived tracing the uppermost (lowest) excitations in each K sector. Due to the finiteness of our system and the rather moderate value $u = 1.5$, PE (IPE) excitations with $K = \pm 3\pi/4$ and π ($K = \pm\pi/4$ and 0) have still finite spectral weight. Since the spectral weight of the PE excitations with $K > \pi/2$ is expected to vanish as N goes to infinity for $u \gg 1$, the lower Hubbard band will be completely filled, and consequently the system behaves as an insulator at $T = 0$. As a result of the coupling to the phonon system the electronic levels in each K sector split, creating phonon side bands. The distinct peaks are separated by multiples of the bare phonon frequency and can be assigned to relaxation processes of the $Q = 0$ phonon modes [23]. The number of phonons involved is controlled by g^2 . $S_{K\sigma}^{\pm}(\omega)$ shows clearly that the total spectral weight of the resulting excitation bands equals the weight of the respective electronic excitations in the pure Hubbard model. Interestingly, mediated by $Q \neq 0$ phonons, there appear “shadows” of the bands composed of a dominant electronic excitation and phonon satellites in a certain K sector (e.g. $K = \pm\pi/2$) in the other K sectors (e.g. $K = \pm\pi/4$). These signatures give rise to a weak “breather-like” excitation being almost dispersionless in the Brillouin zone. The formation of quantum breathers was proposed by W. Z. Wang *et al.* [29], but not doubtless has been detected so far.

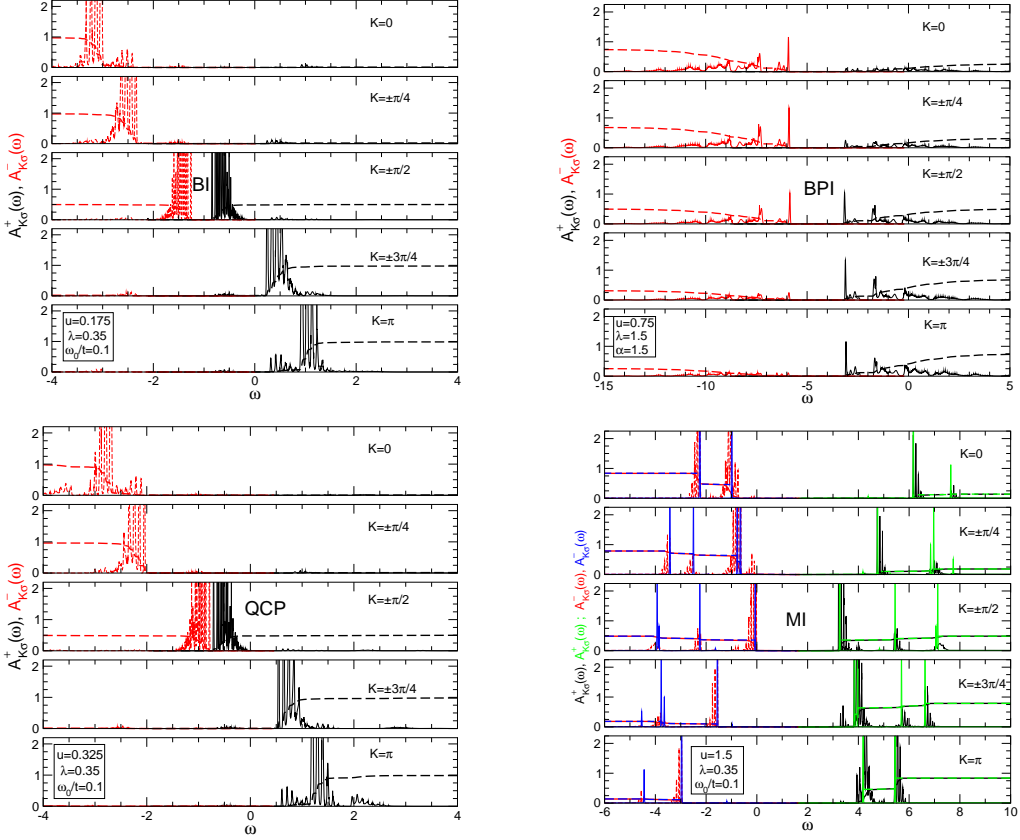


Fig. 10. – Wave-number-resolved spectral densities for photoemission ($A_{K\sigma}^-(\omega)$; dashed (red) lines) and inverse photoemission ($A_{K\sigma}^+(\omega)$; solid (black) lines) obtained by applying our ED-KPM scheme to the HHM. Shown are typical results obtained for the case of a Peierls band insulator (BI) at $\omega_0/t \ll 1$ (left) and bipolaronic insulator (BPI) at $\omega_0/t \gg 1$ (right). The corresponding integrated densities $S_{K\sigma}^{\pm}(\omega)$ are given by dashed lines. The lower panels give the PE and IPE spectra near the PI-MI transition point ($u \simeq 1$) and in the Mott insulating state ($u/\lambda \gg 1$). Data for the pure Hubbard model (blue and green lines) were shifted by $-(\epsilon_p N_e^2/N)$ and included for comparison. Results are taken from Ref. [28].

3.4. Many-body excitation gaps. – Since many-body gaps to excited states form the basis for making contact with experimentally measurable excitation gaps and can also be used to characterise different phases of the HHM, we finally determine the charge and spin gaps,

$$(8) \quad \Delta_c = E_0^{+1}(1/2) + E_0^{-1}(-1/2) - 2E_0(0)$$

$$(9) \quad \Delta_s = E_0(1) - E_0(0) ,$$

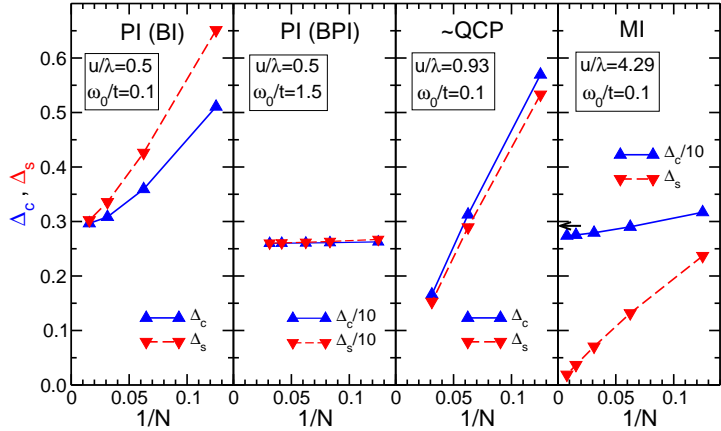


Fig. 11. – DMRG finite-size scaling of spin- and charge excitation gaps in the HHM at $\lambda = 0.35$ and $\omega_0/t = 0.1$). Open and filled symbols denote DMRG results for PBC and OPC boundary conditions, respectively. The accessible system sizes are smaller at larger λ/u , where an increasing number of (phononic) pseudo-sites is required to reach convergence with respect to the phonons. Stars represent the ED results for the eight-site system. The arrow marks the value of the optical gap Δ_{opt} for the Bethe ansatz solvable 1D Hubbard model, which is given by $\Delta_{\text{opt}}/4t = u - 1 + \ln(2)/2u$ in the limit of large $u > 1$ [30].

using DMRG. Here $E_0^{(\pm)}(S^z)$ is the ground-state energy of the HHM at half-filling (with $N_e = N \pm 1$) particles in the sector with total spin- z component S^z .

Obviously, Δ_c and Δ_s are finite in the PI and will converge further to the same value as $N \rightarrow \infty$. Both gaps seem to vanish at the QCP of the HHM with finite-frequency phonons, but in the critical region the finite-size scaling is extremely delicate. In the MI we found a finite charge excitation gap, which in the limit $u/\lambda \gg 1$ scales to the optical gap of the Hubbard model, whereas the extrapolated spin gap remains zero. This can be taken as a clear indication for spin charge separation.

4. – Summary

In this report we have addressed the important problem of quantum phase transitions in one-dimensional strongly coupled electron-phonon systems. As a generic model we analysed the Holstein Hubbard model at half-filling. Applying numerical diagonalisation methods we obtained, by the use of present-day leading-edge supercomputers, basically exact results for both ground-state and spectral properties in the overall region of electron-electron/electron-phonon coupling strengths and phonon frequencies.

For the spinless Holstein model we found that for weak EP couplings the system resides in a metallic (gapless) phase described by two non-universal Luttinger liquid parameters. The renormalised charge velocity and the correlation exponent are obtained by DMRG from finite-size scaling relations, fulfilled with great accuracy. The Luttinger liquid phase splits in an attractive and repulsive regime at low and high phonon fre-

quencies, respectively. Here the polaronic metal, realised for repulsive interactions, is characterised by a strongly reduced mobility of the charge carriers. Increasing the EP interaction, a cross-over between Luttinger liquid and charge density wave behaviour is found. The transition to the CDW state is accompanied by significant changes in the optical response of the system. Most notably seems to be the substantial spectral weight transfer from the Drude to the regular part of the optical conductivity, indicating the increasing importance of inelastic scattering processes in the CDW (PI) regime.

For the much more involved Holstein Hubbard model, with respect to the metal the electron-electron interaction favours a Mott insulating state whereas the EP coupling is responsible for the Peierls insulator to occur (see Fig. 12). True long-range (CDW) order is established in the PI phase only. The PI typifies a band insulator in the adiabatic weak-to-intermediate coupling range or a bipolaronic insulator for non-to-antiadiabatic strong-coupling. Our results for the single-particle spectra indicate that while polaronic features emerge only at strong EP couplings, pronounced phonon signatures, such as multi-phonon bound states inside the CDW gap, can be found in the Mott insulating regime as well. This might be of great importance for interpreting photoemission experiments of low-dimensional materials such as MX-chain compounds. The optical conductivity shows different absorption features in the MI and PI as well and signals that the quantum phase transition between these phases is connected to a change in the ground-state site-parity eigenvalue (of a finite HHM systems with PBC). From our conductivity data we found evidence for only one critical point separating Peierls and Mott insulating phases in the Holstein Hubbard model with dynamical phonons. This differs from the results obtained in the adiabatic limit ($\omega_0 = 0$), where two successive transitions have been detected for weak couplings u , $\lambda \ll 1$ [26]. The Peierls to Mott transition scenario is corroborated by the behaviour of the spin- and charge excitation gaps. From a DMRG finite-size scaling we found $\Delta_c = \Delta_s$ and $\Delta_c > \Delta_s = 0$ in the PI and MI, respectively. The emerging physical picture can be summarised by the phase diagram shown in Fig. 12.

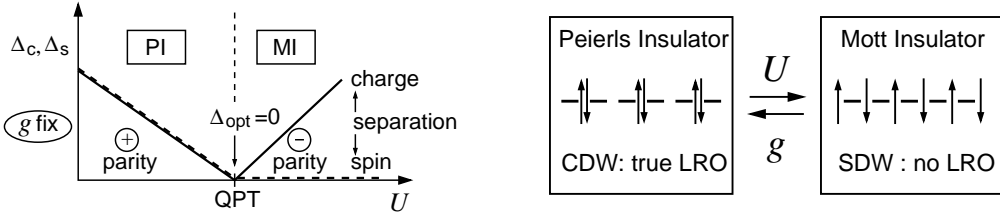


Fig. 12. – Sketch of the PI-MI quantum phase transition in the HHM.

* * *

We would like to thank A. Alvermann, K. W. Becker, A. R. Bishop, H. Büttner, F. Essler, F. Gebhard, F. Göhmann, G. Hager, M. Hohenadler, A. P. Kampf, J. Loos, M. Sekania, S. Sykora, A. Weiße, G. Wellein, and S. R. White for valuable discussions.

REFERENCES

- [1] TSUDA N., NASU K., YANESE A. and SIRATORI K., *Electronic Conduction in Oxides* (Springer-Verlag, Berlin), 1990.
- [2] PEIERLS R., *Quantum theory of solids* (Oxford University Press, Oxford), 1955.
- [3] HOLSTEIN T., *Ann. Phys. (N.Y.)*, **8** (1959) 325; **8** (1959) 343.
- [4] **Fehske H., Alvermann A., Hohenadler M. and Wellein G., Course CLXI, Varenna Proceedings - Editor please update!**
- [5] HUBBARD J., *Proc. Roy. Soc. London, Ser. A*, **277** (1964) 237.
- [6] CAPONE M. and CUCIHI S., *Phys. Rev. Lett.*, **91** (2003) 186405; SANGIOVANNI G., CAPONE M., CASTELLANI C. and CRILLI M., *Phys. Rev. Lett.*, **94** (2005) 026401; **see also their contributions in Course CLXI, Varenna Proceedings - Editor please update!**
- [7] CULLUM J.K. and WILLOUGHBY R.A., *Lanczos Algorithms for Large Symmetric Eigenvalue Computations*, volume I & II, (Birkhäuser, Boston), 1985.
- [8] WELLEIN G., RÖDER H. and FEHSKE H., *Phys. Rev. B*, **53** (1996) 9666.
- [9] SILVER R.N. and RÖDER H., *Phys. Rev. E*, **56** (1997) 4822.
- [10] BÄUML B., WELLEIN G. and FEHSKE H., *Phys. Rev. B*, **58** (1998) 3663; WEISSE A., WELLEIN G., ALVERMANN A. and FEHSKE H., URL <http://arXiv.org/abs/cond-mat/0504627>.
- [11] WHITE S.R., *Phys. Rev. Lett.*, **69** (1992) 2863; HAGER G., JECKELMANN E., FEHSKE H., WELLEIN G. and HAGER G., *J. of Comp. Phys.*, **194** (2004) 795.
- [12] **Jeckelmann E. and Fehske H., Course CLXI Varenna Proceedings - Editor please update!**
- [13] HIRSCH J.E. and FRADKIN E., *Phys. Rev. B*, **27** (1983) 4302.
- [14] BENFATTO G., GALLAVOTTI G. and LEBOWITZ J.L., *Helv. Phys. Acta*, **68** (1995) 312.
- [15] ZHENG H., FEINBERG D. and AVIGNON M., *Phys. Rev. B*, **39** (1989) 9405.
- [16] CARON L.G. and BOURBONNAIS C., *Phys. Rev. B*, **29** (1984) 4230.
- [17] MCKENZIE R.H., HAMER C.J. and MURRAY D.W., *Phys. Rev. B*, **53** (1996) 9676.
- [18] WEISSE A. and FEHSKE H., *Phys. Rev. B*, **58** (1998) 6208.
- [19] BURSILL R.J., MCKENZIE R.H. and HAMER C.J., *Phys. Rev. Lett.*, **80** (1998) 5607; FEHSKE H., WELLEIN G., HAGER G., WEISSE A., BECKER K.W. and BISHOP A.R., *Physica B*, **359-361** (2005) 699.
- [20] HALDANE F.D.M., *Phys. Rev. Lett.*, **45** (1980) 1358.
- [21] CARDY J.L., *J. Phys. A*, **17** (1984) L385; VOIT J., *Rep. Prog. Phys.*, **58** (1997) 977.
- [22] HOHENADLER M., WELLEIN G., BISHOP A.R., ALVERMANN A. and FEHSKE H., 2005, URL <http://arXiv.org/abs/cond-mat/05xxxxxx>.
- [23] SYKORA S., HÜBSCH A., BECKER K.W., WELLEIN G. and FEHSKE H., *Phys. Rev. B*, **71** (2005) 045112.
- [24] MEYER D., HEWSON A.C. and BULLA R., *Phys. Rev. Lett.*, **89** (2002) 196401; **Hewson A.C., Course CLXI Varenna Proceedings - Editor please update!**
- [25] JECKELMANN E., ZHANG C. and WHITE S.R., *Phys. Rev. B*, **60** (1999) 7950.
- [26] FEHSKE H., KAMPF A.P., SEKANIA M. and WELLEIN G., *Eur. Phys. J. B*, **31** (2003) 11.
- [27] KOHN W., *Physical Review*, **133** (1964) A171.
- [28] FEHSKE H., WELLEIN G., HAGER G., WEISSE A. and BISHOP A.R., *Phys. Rev. B*, **69** (2004) 165115.
- [29] WANG W.Z., BISHOP A.R., GAMMEL J.T. and SILVER R.N., *Phys. Rev. Lett.*, **80** (1998) 3284.
- [30] OVCHINNIKOV A.A., *Sov. Phys. JETP*, **30** (1970) 1160.